NON-NEWTONIAN TEMPERATURE AND PRESSURE EFFECTS OF A POWDER LUBRICANT SLURRY IN A ROTATING HYDROSTATIC STEP BEARING

BY

WILLIAM EDWARD FINN

A THESIS PRESENTED TO THE GRADUATE SCHOOL
OF THE UNIVERSITY OF FLORIDA IN PARTIAL FULFILLMENT
OF THE REQUIREMENTS FOR THE DEGREE OF
MASTER OF SCIENCE

UNIVERSITY OF FLORIDA

1993

ACKNOWLEDGMENTS

I am very grateful for the support provided by the following individuals:

Dr. D.W. Dareing first interested me in the tribology area and was instrumental in guiding my research. He helped refine the initial problem statement that became my master's thesis.

Dr. J.E. Peterson devoted many hours obtaining funding, providing counsel, solving experimental setbacks and supervising my research. Her encouragement and assistance were critical to the timely completion of this thesis.

Dr. J.K. Schueller's motivation and interest kept the project moving and provided additional reference material for this project.

Finally, the test rig modifications would not have been possible without the technical assistance from Mr. Steve Sowa and his division's machining work, material from Mr. Howard Purdy and Mr. Jeff Studstill and electrical guidance and material from Mr. Robert Harker.

TABLE OF CONTENTS

NOMENCLATURE

A.....Area of bearing surface, in^2
A,B...Linear regression coefficients
b.....Width of flow, in
C.....Fluid specific heat, Btu/lbs·°F
C_1....Constant of integration
C_2....Constant of integration
E_f....Frictional energy loss, in·lbs/sec
E_p....Pump energy loss, in·lbs/sec
F.....Force, lbs
h.....Film thickness, in
J.....Conversion factor, ft·lbs/Btu
K.....Power Law constant, $Pa \cdot sec^n$
K_0....Bingham and Hyperbolic model constant, Pa·sec
M.....Frictional torque, in·lbs
N.....Angular velocity, RPM
n.....Power Law exponent
P.....Pressure, lbs/in^2
P_s....Supply pressure, lbs/in^2
ΔP....Pressure difference across bearing, lbs/in^2
Q.....Flow rate, in^3/sec
R.....Outside radius, in
R_o....Step radius, in
R_1....Thermister one resistance, kOhms
R_2....Thermister two resistance, kOhms
R_e....Reynolds number, $\frac{vh}{\nu}$, Nondimensional
r.....Radius value between R_o and R, in
T.....Temperature, Rankine
T_0....Baseline temperature, Rankine
T_1....Thermister one temperature, Rankine
T_2....Thermister two temperature, Rankine
ΔT....Temperature difference, °F
v.....Fluid velocity, in/sec
v(y)..Fluid velocity, in/sec
$\frac{\partial h}{\partial y_i}$....Partial derivative of film thickness
γ.....Fluid weight density, lbs/in^3

γ.....Power Law model shear rate, dv/dy
μ.....Fluid viscosity, reyns
σ_y....Standard deviation along y-axis
τ.....Shear stress, lbs/in^2
τ_0....Bingham and Hyperbolic model yield point, Pa
τ_N....Newtonian shear stress, lbs/in^2
τ_{Non-N}..Non-Newtonian shear stress, lbs/in^2
ν.....Kinematic fluid viscosity, in^2/sec
ω.....Angular velocity, rad/sec
ω_h....Uncertainty

Abstract of Thesis Presented to the Graduate School
of the University of Florida in Partial Fulfillment of
the Requirements for the Degree of Master of Science

NON-NEWTONIAN TEMPERATURE AND PRESSURE EFFECTS
OF A POWDER LUBRICANT SLURRY IN A
ROTATING HYDROSTATIC STEP BEARING

By

William Edward Finn

May 1993

Chairperson: Dr. J.E. Peterson
Major Department: Mechanical Engineering

The purpose of this research was to investigate the pressure and temperature effects of graphite powder lubricant added to a carrier fluid of ethylene glycol as applied in a rotating hydrostatic step bearing. After the testing apparatus was designed and modified, the temperature and pressure profiles were determined analytically and experimentally.

The rheological behavior of the non-Newtonian lubricant was modeled using a Power Law model developed previously. This model has been proven to match experimental data and

was therefore the tool used for comparison with research data.

Ethylene glycol was used as the Newtonian lubricant for the initial experimentation, which provided a check on the test apparatus and a comparison with the non-Newtonian graphite slurry.

The measured data for the temperature increase dependency on rotation for both fluids compared favorably to the mathematical predictions. A significantly higher temperature difference was seen in the non-Newtonian lubricant due to the higher shear rates.

The pressure profile, while not directly dependent on rotation as shown in the mathematical model, demonstrated a reduction based upon higher rotation speeds. This reduction was greater for the non-Newtonian lubricant. Due to the higher temperatures seen in the non-Newtonian lubricant and temperature dependent Power Law constants, a pressure loss is expected. For the Newtonian lubricant, viscosity is dependent upon fluid temperature.

Therefore, the effects of operating speed and temperature on a non-Newtonian lubricant should be considered, as well as their greater load-carrying capacity.

CHAPTER 1
BACKGROUND AND SIGNIFICANCE OF RESEARCH

Background of Hydrostatic Bearings

Hydrostatic bearings were first demonstrated in 1851 by L.D. Girard through an invention involving high pressure water-fed bearings used for a railway propulsion system and patented in 1865 (1, p. 225; 2, p. 435). This externally pressurized or hydrostatic system was further demonstrated at the 1878 Paris Industrial Exposition when a heavy block with four feet was floated on a thin film of lubricant that was pumped down each leg (1, 2). The first analysis of a thrust bearing was provided by Lord Rayleigh in 1917 using the hydrostatic system and solving the load, flowrate and frictional torque (1; 2, p. 436).

Current applications include the analysing magnet of the Nuclear Structure Facility at the SERC Daresbury Laboratory (1, p. 227), the Halle optical telescope (2, p. 436), the 210-foot-diameter tracking antenna at the NASA-Jet Propulsion Laboratory Deep Space Instrumentation Facility (3, p. 33-51), and Denver's Mile High Stadium (4, p. 78).

All applications involve moving extreme weight with minimal effort and in some cases, high precision. In 1972, the Institution of Mechanical Engineers published proceedings on a conference solely devoted to externally pressurized bearings (2, p. 437). Since that time, more effort has been spent by industry on the study of the lubricants as most of the basic mechanical principles of the hydrostatic bearing had been solved.

Significance of the Research

The addition of solid lubricants to Newtonian fluids has been the subject of extensive research. One major reason for the addition of solid lubricants is the greater stability of these mixtures when subjected to extreme temperatures. The aerospace industry, military, and NASA all report using solid lubricants because of their greater load and temperature capabilities (5, p. 5; 6, p. 5, 83-86). Many commercial applications exist for a Graphite/Glycol lubricant mixture including switch gear equipment and high temperature oven bearings (5, p. 85-86).

The U.S. gas turbine industry has started a new program in cooperation with NASA and the Department of Defense called the Integrated High Performance Turbine Engine

Technology (IHPTET) program (7, p. 114). The desired double propulsion capability from the large speeds in the gas turbine shafts result in high temperatures which have further emphasized the requirement for nontraditional lubricants. The approximate working temperatures of different types of lubricants are as follows (8, p. 2):

Petroleum Lubricants	below 100°C
Synthetic Lubricants	200 to 315°C
Powder Lubricants	425 to 675°C

The powder lubricant is supplied to the system through pressurized air or slurries containing the powder (7, p. 114). These non-Newtonian lubricants are the subject of current research towards more accurate behavior prediction.

CHAPTER 2
OBJECTIVE OF THE RESEARCH

This research investigates the pressure and temperature affects of graphite powder lubricant added to a carrier fluid of ethylene glycol as applied in a rotating hydrostatic step bearing. The graphite powder was provided by Union Carbide and the ethylene glycol was provided by Fisher Scientific. The methodology included laboratory testing and mathematical modeling for comparison with the experimental results.

An existing laboratory test rig was extensively modified to impart an angular velocity to a hydrostatic step bearing and to measure temperature, pressure, flowrate, revolutions per minute (RPM), and film thickness. Measurements for the ethylene glycol were obtained for use as a check on the testing rig and for establishing baseline data.

The goal was to formulate temperature equations dependent upon the rotational velocity and compare this affect with the pressure distribution across the bearing

radius. Potential inertial affects from the step bearing's rotation and its effects on the graphite particles in the ethylene glycol would also be examined in the pressure profile.

An understanding of these fundamental lubrication principles in a non-Newtonian fluid is necessary for developing a powder lubricant slurry approach in future applications.

CHAPTER 3
RESEARCH EQUIPMENT AND METHOD

Laboratory Test Equipment

The laboratory testing was an important portion of this research. Significant time and effort was spent designing, fabricating, and redesigning the modifications to the existing test rig. The modified hydrostatic test rig (Figure 3-1) contains a flat base and a parallel hydrostatic step bearing (items 5 and 6, Figure 3-1). The bearing consisted of an upper surface with an outside diameter of four inches and an inside diameter of two inches. It was connected to the shaft and gear assembly through a ball bearing assembly designed and fabricated to maintain a parallel surface to the base while rotating. The resultant constant film thickness was measured by three LVDT displacement sensors (item 4, Figure 3-1) mounted on supports which were placed 120 degrees apart on top of the hydrostatic step bearing. Since three points define a plane, the use of three sensors was sufficient. The voltage

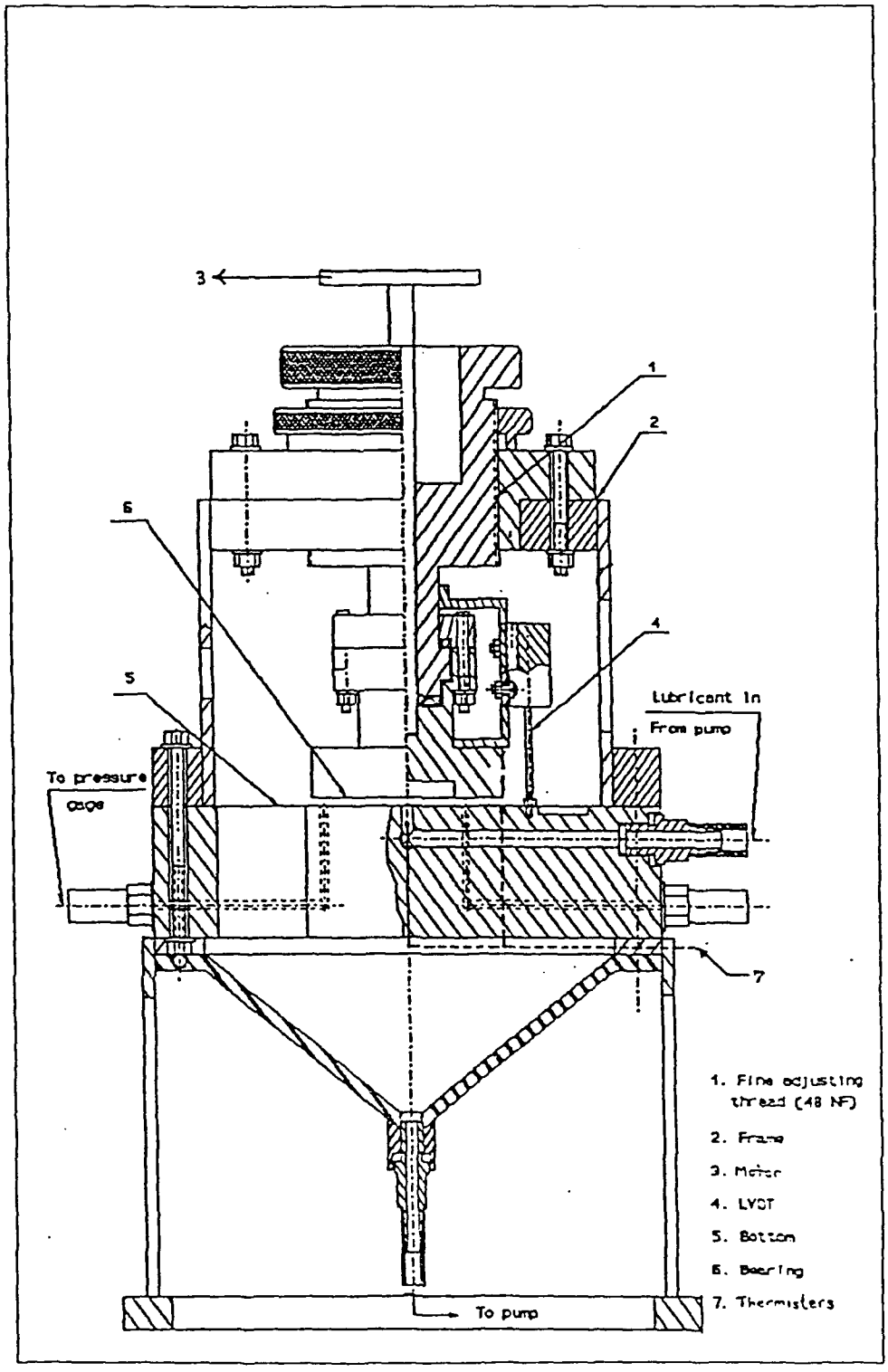

Figure 3-1. Modified Hydrostatic Test Rig

reading of the LVDT displacement sensors was compared to the calibration and provided film thickness. The specifications for the LVDT sensors are as follows:

Make	Trans-Tek, Inc.
Model	DC-DC Series 240 02141-0000
Input Volts DC (v)	6 to 30
Linearity %	.5
Freq. Response 3dB down	140 Hz
Temperature Range	-50 C to 120 C
Resolution	Infinite

The film thickness could be adjusted through the fine adjusting thread (item 1, Figure 3-1) that connected the screw shaft to the frame (item 2, Figure 3-1). The gear assembly was belt driven by a controllable, variable speed motor (item 3, Figure 3-1). The RPM was measured directly through a Pioneer Digital Photo tachometer, model DT-36. The motor specifications are as follows:

Make	Dayton Permanent Magnet DC
Model	2M168B
HP	1/2
RPM	1725
Armature Volts	90 VDC
Armature Current	5.5 amps

Two thermisters were installed in the base of the bearing surface (item 7, Figure 3-1) and measured the temperature of the lubricant entering the recess pocket and at the perimeter of the hydrostatic step bearing. The

measured resistance was compared to the thermister's calibration and provided the temperature.

The lubricant was supplied to the bearing surfaces by an external pump through an internal orifice. The pump's flow rate was adjustable. It's specifications are as follows:

Make	Micropump Corp.
Model	415
Motor/Pump Coupling	Magnetic Drive
Maximum Flow Rate	630 ml/min
Rated Maximum Pressure	20 psi

The fluid flow was routed through a rotameter flow meter. Comparing the reading with the flow meter's calibration provided the flow rate.

The fluid film pressures were measured with dial pressure gages at four locations across the bearing surface located:

1) within the recess pocket
2) 1/4 inch from the inside pocket
3) 1/2 inch from the inside pocket
4) 3/4 inch from the inside pocket

Research Method

The experimental test rig was used to determine the effects of powder lubricants in a carrier fluid subjected to rotation in a hydrostatic step bearing. The testing method

is described in Chapter 5. First, the various measuring devices were calibrated.

Uncertainty Analysis and Calibration

The uncertainty analysis for the flowmeter, thermister, and LVDT data was calculated using a least squares fit technique to determine the deviation width. Since each curve fit was linear, the formula (9, p. 158) used to determine the standard deviation is written as equation (3-1) where the coefficients A and B are determined through the linear regression curve fit. Further, σ_y was multiplied by 1.7 in order to obtain 10:1 odds or a 90% probability that a measurement will fall within 1.7 standard deviations.

$$\sigma_y^2 = \frac{1}{N-2}\Sigma(y_i - A - Bx_i)^2 \qquad (3\text{-}1)$$

The rotameter flowmeter was calibrated by adjusting the flowrate through the pump, marking the flowmeter reading, and timing the fill time of the liquid into a beaker of known volume. A linear regression or least-squares fit (9, p. 154) for a line of the measured data provided the calibration equation:

$$y = 5.55x - 205.69 \qquad (3\text{-}2)$$

where y is the flow rate in ml/min and x is the flowmeter reading. The calibration curve is shown in figure 3-2. The flowmeter uncertainty calculated through equation (3-1) for both liquids was ±11.8 ml/min.

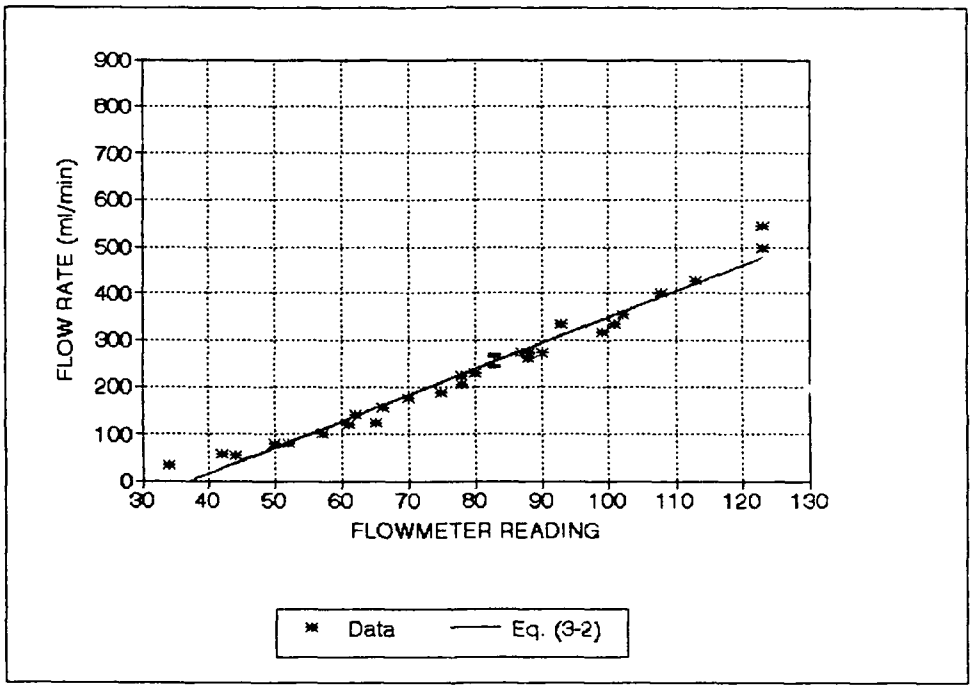

Figure 3-2. Flowmeter calibration curve

The thermisters were calibrated by placing them in a water bath, adjusting the temperature, reading the mercury thermometer temperature, and recording the thermisters' resistance. The uncertainty of the thermometer using half the least count was ±0.1°F. Thermisters function on a

principle that their resistance is lower at higher temperatures. This dependency is logarithmic and shown by the equation:

$$\log\left(\frac{R}{R_o}\right) = B\left(\frac{1}{T} - \frac{1}{T_o}\right) + A \qquad (3\text{-}3)$$

where R_o and T_o are the baseline resistance in kOhms and temperature in Rankine, respectively. The constants A and B were determined through calibration for the two thermisters using linear regression. Rearranging the results and solving for resistance as a function of temperature provided the calibration equations:

$$R_1 = 11.247\left(10^{3083.39\left(\frac{1}{T_1} - \frac{1}{532.47}\right) - .00092}\right) \qquad (3\text{-}4)$$

$$R_2 = 11.56\left(10^{3112.86\left(\frac{1}{T_2} - \frac{1}{532.47}\right) - .00027}\right) \qquad (3\text{-}5)$$

where R_1, T_1 and R_2, T_2 are the resistances and temperatures of thermisters one and two, respectively. The calibration curves are shown in figures 3-3 and 3-4. Their uncertainty calculated through equation (3-1) was ± 1 Ohm (.001 kOhms).

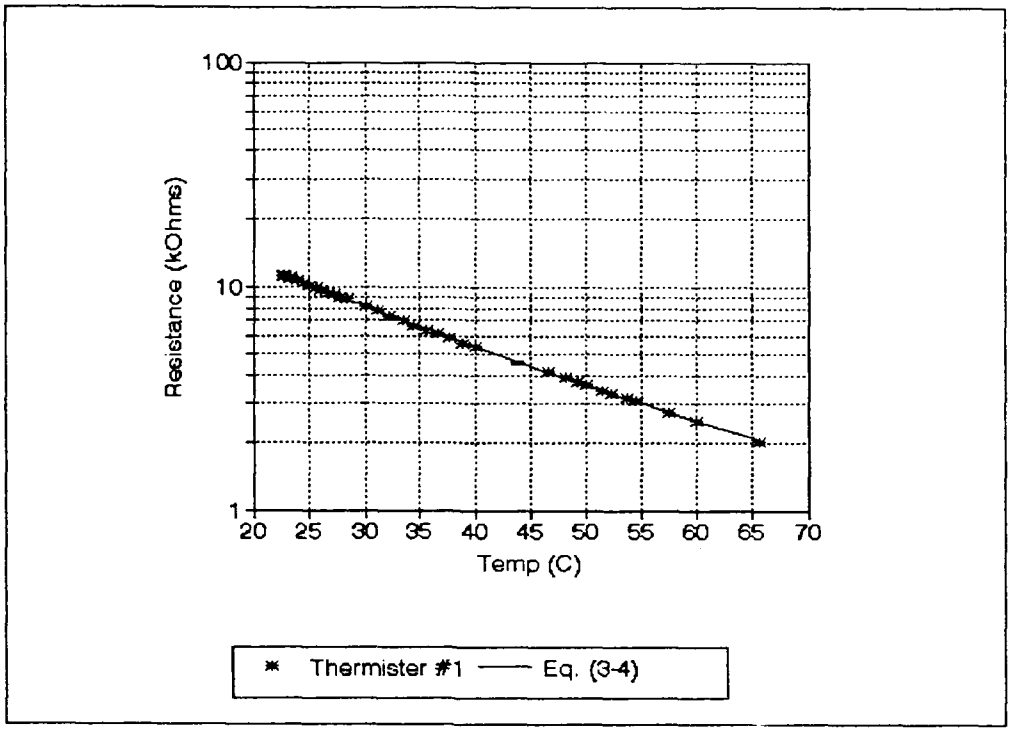

Figure 3-3. Thermister One calibration curve

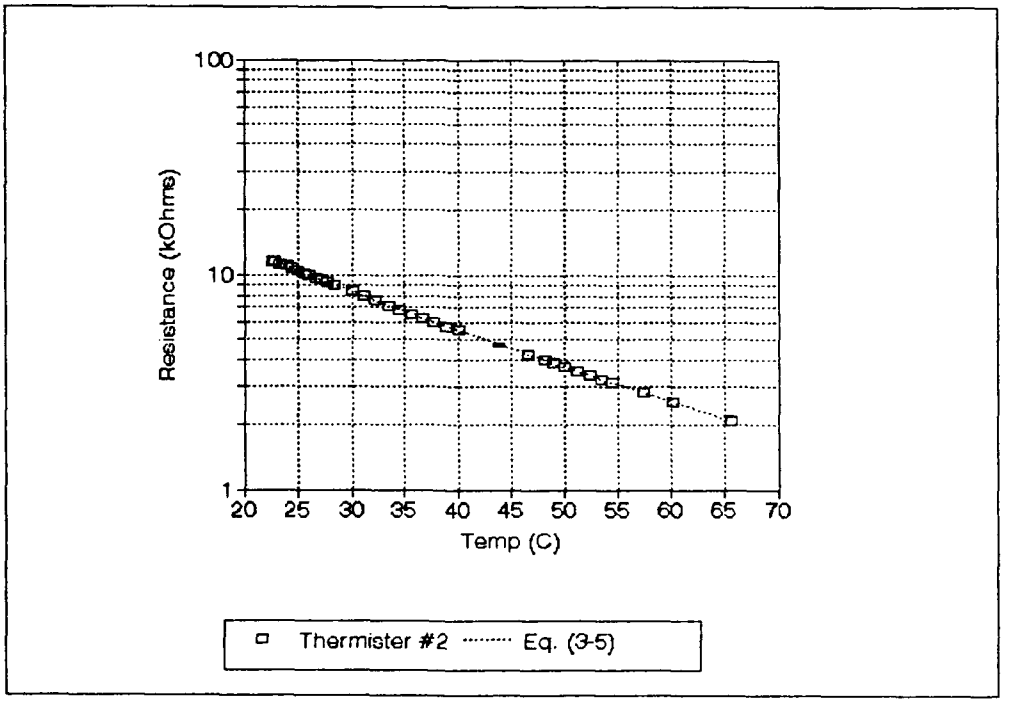

Figure 3-4. Thermister Two calibration curve

The LVDTs were calibrated by unscrewing the shaft of known adjusting thread through equidistant intervals beginning at zero when the hydrostatic step bearing was touching the flat base. The voltage reading of each LVDT was recorded at these intervals. Linear regression of the measured data for each LVDT provided the following calibration equations:

LVDT A: $$y_A = -148.4x_A + 19.44 \quad (3\text{-}6)$$

LVDT B: $$y_B = -133.8x_B + 19.78 \quad (3\text{-}7)$$

LVDT C: $$y_C = -97.6x_C + 19.97 \quad (3\text{-}8)$$

where y is the LVDT reading in volts and x is the film thickness in inches. The calibration curves are shown in figure 3-5. The uncertainty calculated through equation (3-1) was ±0.04 volts for LVDT A, ±0.07 volts for LVDT B, and ±0.05 volts for LVDT C.

The uncertainty for the tachometer was ±1 RPM as given by the manufacturer. It was verified by repeatedly setting the maximum RPM value and noting that the value was consistently within ±1 of 670 RPM. The uncertainty for the

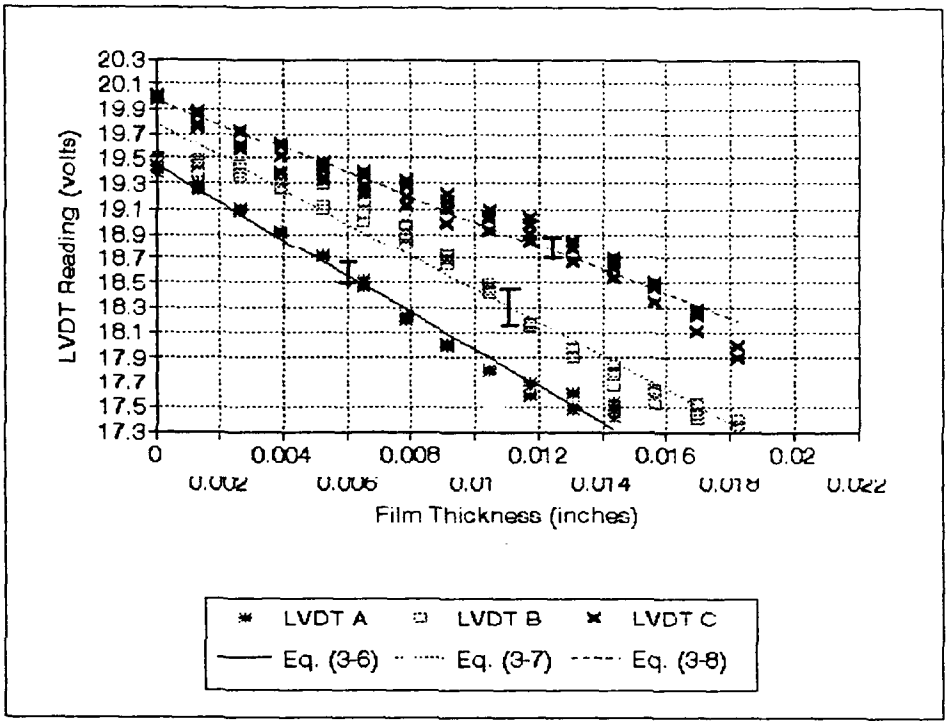

Figure 3-5. LVDT calibration curves

dial pressure gages was ±0.5 psi using half the least count.

The film thickness, h, was calculated as an average of the three LVDT readings. In order to determine the overall uncertainty of the film thickness during the testing, equations (3-6), (3-7), and (3-8) were rearranged to solve for film thickness based upon LVDT voltage. The three equations were averaged resulting in

$$h = \frac{x_A + x_B + x_C}{3} = -.0022y_A - .0025y_B - .0033y_C + .161 \quad (3\text{-}9)$$

A root-sum-square method (9, p. 73; 10, p. 15; 11, p. 254) was employed as shown in equation (3-10) where h is determined from equation (3-9) and $\frac{\partial h}{\partial y_i}$ is its partial derivative with respect to LVDT A, B, or C. The uncertainty of LVDT A, B, or C is ω_i as derived earlier.

$$\omega_h = \left\{ \sum \left(\frac{\partial h}{\partial y_i} \omega_i \right)^2 \right\}^{1/2} \qquad (3\text{-}10)$$

The overall uncertainty of h, the film thickness, was ±0.0003 inches. This is important because the film thickness in the mathematical modeling of the pressure profile is raised to the third power resulting in a three times greater uncertainty.

CHAPTER 4
MATHEMATICAL MODELING

The mathematical calculations in this chapter were formulated in order to model the temperature change and the pressure profile in a hydrostatic step bearing while varying the film thickness and revolutions per minute (RPM). The comparisons of the measured data with the mathematical modeling are discussed in Chapter 5.

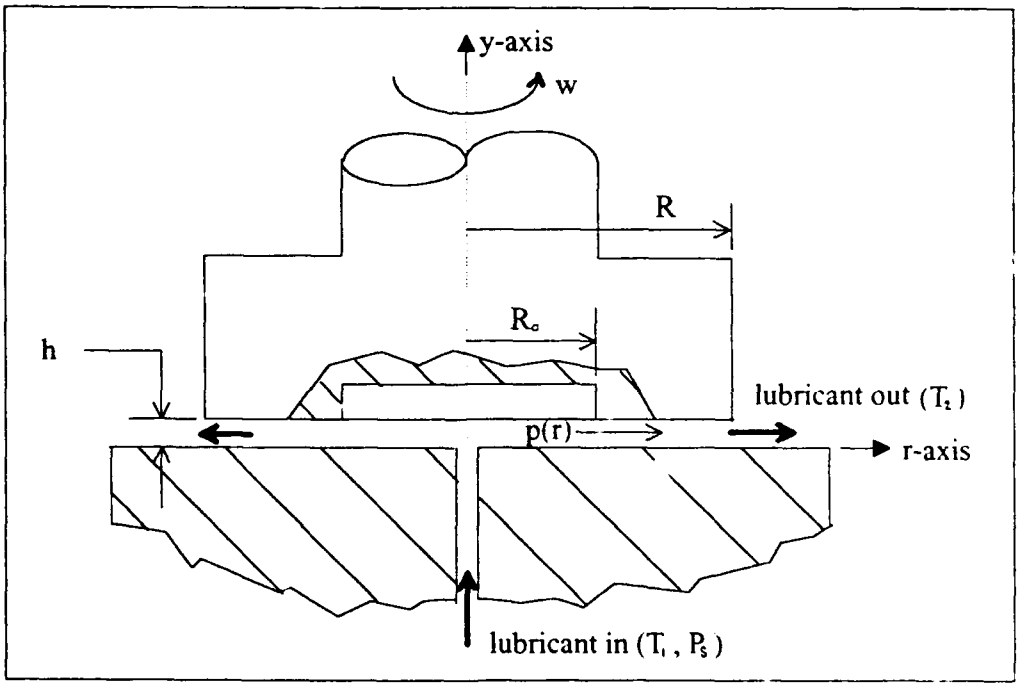

Figure 4-1. Schematic of Hydrostatic Step Bearing

The equations derived for the temperature and pressure relationships of the hydrostatic step bearing shown in figure 4-1 involve some basic assumptions (4, pp. 80-88; 8, p. 10):

1. The flow is laminar. The maximum Reynolds number using the greatest flow rate and the radius at the step is 25.9. A Reynolds number less than 1000 in bearing applications is assumed to be laminar flow (4, p. 63; 12, p. 343-346). The flow is pressure induced.
2. The inertial forces resulting from the rotation of the bearing are negligible when compared to the viscous shear forces and can be neglected.
3. The fluids are incompressible.
4. The pressure is a function of the radius, neglecting any side leakage.
5. The temperature is constant across the film thickness.
6. All the heat generated appears in the fluid and corresponds to its temperature rise.
7. The pressure at the outside of the bearing is assumed to be ambient.

Temperature Equations

Because of the different properties of Newtonian and non-Newtonian fluids, two different mathematical model relations were used.

Ethylene Glycol Relations

Pure ethylene glycol is a Newtonian fluid and therefore, the following relations apply according to the geometry of the test rig as shown in the schematic (figure 4-1).

The pump loss is given by the relation (4, p. 86),

$$E_p = Q\Delta P \tag{4-1}$$

where Q is the flow rate in cubic inches per second, ΔP is the pressure difference in psi, and E_p is energy in inch-pounds per second. The friction loss on the bearing due to rotation can be solved beginning with Newton's fluid friction law,

$$\tau_N = \mu \frac{dv}{dy} \tag{4-2}$$

Referring to Figure 4-1 and substituting the film thickness, h, for the differential width, this is equivalent to Newton's equation of viscous friction drag,

$$F = \mu A \frac{v}{h} \tag{4-3}$$

Substituting πr^2 for A and considering a differential annulus results,

$$dF = \mu \frac{v}{h}(2\pi r dr) \tag{4-4}$$

When one of the contacting surfaces is stationary, $v=\omega r$, where ω is the angular velocity in radians per second. Multiplying both sides by r to determine the torque on an elemental annulus of radius r and width dr is

$$rdF = dM = \frac{2\pi\mu\omega}{h} r^3 dr \tag{4-5}$$

The total frictional torque (4, p. 88) becomes

$$M = \frac{2\pi\mu\omega}{h} \int_{R_o}^{R} r^3 dr = \frac{2\pi\mu\omega}{h}\left[\frac{R^4 - R_o^4}{4}\right] \tag{4-6}$$

where μ is the viscosity in reyns, ω is the angular velocity in radians per second, h is the film thickness in inches, R_o is the radius to the step in inches, and R is the radius to the outside edge of the bearing in inches.

The friction loss is given by the equation (4, p. 88)

$$E_f = \frac{2\pi MN}{60} \qquad (4\text{-}7)$$

where E_f is energy in inch-pounds per second, N is the rotation in revolutions per minute (RPM), and M is the torque in inch-pounds. Therefore, the total energy loss across the bearing from r=o to r=R can be expressed as follows (4, p. 90),

$$E_T = E_p + E_f = 12JQ\gamma C\Delta T \qquad (4\text{-}8)$$

where 12J is the conversion factor for foot-pounds to British thermal units (Btu), Q is the flow rate of the fluid in cubic inches per second, γ is the weight density of the fluid in pounds per cubic inches, C is the specific heat of the fluid in Btu per pounds-°F, and ΔT is the temperature difference across the bearing in °F. The temperature

difference can be solved for as a function of the rotation since the flow rate, pressure difference, and film thickness are held constant. The pressure difference from r=0 to r=R equals the supply pressure since the pressure at the outside of the bearing, P(R), is assumed to be ambient. Therefore, substituting the values for E_r and E_p and rearranging to solve for ΔT results

$$\Delta T = \frac{P_s}{12J\gamma C} + \frac{\pi^3 N^2 \mu \left(R^4 - R_o^4\right)}{21600 JQ\gamma Ch} \qquad (4\text{-}9)$$

Graphite/Ethylene Glycol Relations

A mixture of ethylene glycol and graphite powder is a non-Newtonian fluid and requires different fundamental modeling. Currently, there are three accepted rheological models (7, pp. 115-116; 8, p. 15). First, the Bingham model is stated:

$$\tau_{Non-N} = \tau_o + K_o \gamma \qquad (4\text{-}10)$$

where τ_{Non-N} is the non-Newtonian shear stress in Pascals, τ_o is the yield point in Pascals, K_o is the Bingham

constant in Pascal-seconds, and γ is the shear rate in seconds^{-1}. This model has shown to deviate significantly from measurements at low shear rates, however, it is accurate at high shear rates where many lubricant films operate (7, p. 115). Second, the Hyperbolic model is stated:

$$\tau_{Non-N} = \left[(K_o \gamma)^2 + 2K_o \tau_o \gamma \right]^{1/2} \qquad (4\text{-}11)$$

where the shear stress, yield point, Bingham constant, and shear rate variables are the same as the Bingham model. This function is similar to the Bingham model at high shear rates and has proven to match better with results at low shear rates (7, p. 116).

Finally, the Power Law model is stated:

$$\tau_{Non-N} = K\gamma^n \qquad (4\text{-}12)$$

where τ_{Non-N} is the non-Newtonian shear stress in Pascals, K is the Power Law constant in Pascal-seconds^n, γ is the shear rate in seconds^n, and n is a nondimensional Power Law constant. This model has proven useful for

describing shear stress-shear rate relations for non-Newtonian fluids without a yield point and is useful for fluid flow formulations (7, p. 116).

Since it has been shown that the Power Law model can reasonably model a 1:8 ratio of graphite powder to ethylene glycol (7, p. 116; 8, pp. 31-32; 13, pp. 86-87) and the mathematical expression is uncomplicated to evaluate, it was used in this research.

Table 4-1. Power Law Constants

Graphite-Ethylene Glycol (1:8)		
Temp, °C	K, Pa-sec^n	n
20	0.0572	0.973
30	0.0448	0.971
40	0.039	0.969
50	0.0361	0.969

The Power Law constants used were taken from Table 4-1 (7, p. 116) dependent on the temperature of the fluid.

The pump loss given by equation (4-1) is still applicable. The friction loss on the bearing due to

rotation can be determined beginning with the Power Law model, equation (4-12), rewritten as follows:

$$\tau = K\left(\frac{dv}{dy}\right)^n \qquad (4\text{-}13)$$

This is equivalent to the equation of viscous friction drag,

$$F = KA\left(\frac{v}{h}\right)^n \qquad (4\text{-}14)$$

Substituting πr^2 for A and considering a differential annulus results,

$$dF = K\left(\frac{v}{h}\right)^n (2\pi r dr) \qquad (4\text{-}15)$$

Since one of the contacting surfaces is stationary, $v=\omega r$, where ω is the angular velocity in radians per second. Multiplying both sides by r to determine the torque on an elemental annulus of radius r and width dr results,

$$rdF = dM = 2\pi K\left(\frac{\omega}{h}\right)^n (r^{n+2} dr) \qquad (4\text{-}16)$$

The total frictional torque becomes

$$M = 2\pi K\left(\frac{\omega}{h}\right)^n \int_{R_o}^{R} (r^{n+2})dr$$

$$M = 2\pi K\left(\frac{\omega}{h}\right)^n \left[\frac{R^{n+3} - R_o^{n+3}}{n+3}\right] \qquad (4\text{-}17)$$

This is equivalent to equation (4-6) for the Newtonian fluid where n=1 and K is the viscosity. A conversion factor is necessary since the Power Law constant, K, has units of Pascals versus pounds per square inch (psi). The friction loss from equation (4-7) expands to the following:

$$E_f = \frac{\pi^2 KN}{15}\left(\frac{\pi N}{30h}\right)^n \left[\frac{R^{n+3} - R_o^{n+3}}{n+3}\right] \qquad (4\text{-}18)$$

Therefore, the total energy loss from r=0 to r=R can be determined according to equation (4-8). The temperature difference is solved as a function of the rotation since the flow rate, pressure difference, and film thickness are held constant. The pressure difference from r=0 to r=R equals the supply pressure since the pressure at the outside of the bearing, P(R), is assumed to be ambient. Therefore,

substituting the values for E_f and E_p and rearranging to solve for ΔT results

$$\Delta T = \frac{P_s}{12J\gamma C} + \frac{\pi^2 KN}{1240200JQ\gamma C}\left(\frac{\pi N}{30h}\right)^n\left[\frac{R^{n+3}-R_o^{n+3}}{n+3}\right] \qquad (4\text{-}19)$$

Pressure Equations

The different properties for Newtonian and non-Newtonian fluids required different mathematical model relations for each as previously discussed in the

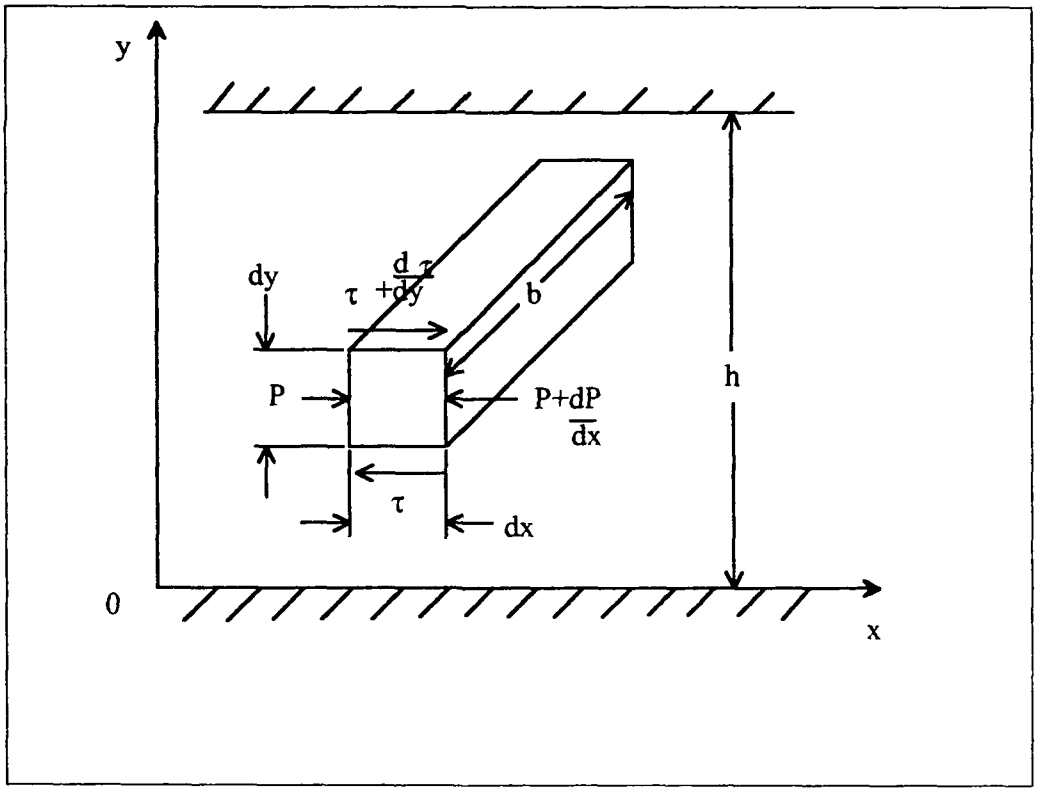

Figure 4-2. Pressure distribution on a unit volume

derivations of equations (4-2) and (4-12). The fluid flow in the hydrostatic step bearing is pressure induced.

Ethylene Glycol Relations

For the geometry of the hydrostatic step bearing (Figure 4-1), the pressure distribution on a unit volume is shown in Figure 4-2.

Summing the forces in the horizontal direction and rearranging is

$$\frac{dP}{dx} = \frac{d\tau}{dy} \qquad (4\text{-}20)$$

Substituting equation (4-2), it is a simplified form of the Navier-Stokes equations (12, p.343) for pressure induced flow between two parallel surfaces,

$$\frac{dp}{dx} = \mu \frac{\partial^2 v}{\partial y^2} \qquad (4\text{-}21)$$

Integrating twice across the y direction, assuming dp/dx is a constant across the film thickness, yields

$$v(y) = \frac{1}{2\mu}\frac{dp}{dx}y^2 + C_1 y + C_2 \qquad (4\text{-}22)$$

Evaluating the constants of integration, C_1 and C_2, with the boundary conditions that v(0)=0 and v(h)=0 results

$$v(y) = \frac{1}{2\mu}\frac{dp}{dx}(y^2 - yh) \qquad (4\text{-}23)$$

Solving for the flow rate, Q, is shown

$$Q = \int_0^h v(y)dyb \qquad (4\text{-}24)$$

Integrating, it is stated (4, p. 81; 7, p. 118; 8, p. 12)

$$Q = \frac{bh^3}{12\mu}\frac{dp}{dx} \qquad (4\text{-}25)$$

where Q is the flow rate in cubic inches per second, b is the plate width in inches, h is the film thickness in inches, μ is the viscosity in reyns, and dp/dx is the pressure gradient. Equation (4-25) is commonly used in radial flow situations. Since ethylene glycol is a Newtonian fluid, Replacing b by 2πr, dx by dr, integrating and solving for the pressure at any radius, r, becomes (4, p. 82; 8, p.14; 14, p. 7)

$$P = \frac{6\mu Q}{\pi h^3} \ln \frac{R}{r} \qquad (4\text{-}26)$$

where P is the pressure at any point along the radius in pounds per square inch (psi), R is the outside radius of the bearing, r is any radius between R_o and R, Q is the flow rate in cubic inches per second, h is the film thickness in inches, and μ is the viscosity in reyns.

Graphite/Ethylene Glycol Relations

Using the same assumptions as the ethylene glycol relations with the exception of equation (4-12) for the Power Law Model described earlier, it is stated (7, p. 118; 8, p. 16; 14, p. 7)

$$Q = 2b\left(\frac{1}{K}\frac{dp}{dx}\right)^{\frac{1}{n}}\left(\frac{h}{2}\right)^{\frac{2n+1}{n}}\left(\frac{n}{2n+1}\right) \qquad (4\text{-}27)$$

Replacing b by 2πr, dx by dr, integrating and solving for the pressure at any radius, r, becomes (8, p. 16; 14, p. 8)

$$P = Q^n K\left(\frac{2n+1}{4\pi n}\right)^n\left(\frac{2}{h}\right)^{2n+1}\left(\frac{R^{1-n}-r^{1-n}}{1-n}\right) \qquad (4\text{-}28)$$

The Power Law constants, K and n, are determined from table 4-1 for equations (4-22) and (4-23) dependent upon the temperature of the fluid.

For this research, the pressure values for both fluids were nondimensionalized by dividing by the inlet supply pressure. The flow rate and film thickness were constant so that the RPM could be adjusted in order to observe the rotational effects on the pressure at the set points along the radius.

CHAPTER 5
EXPERIMENTAL RESULTS

Experimental Method

The initial testing with the laboratory test rig was performed with pure ethylene glycol as the lubricant. This data provided a check on the instruments and equipment and a comparison for studying the effects of adding graphite powder to the ethylene glycol.

The film thickness was set based upon the LVDT readings. The flow rate of the lubricant was adjusted so that the maximum pressure of the dial gages would not be exceeded. The motor was energized and readings were taken of the LVDT voltages, flowmeter, pressure gages, and thermisters as the rotation was adjusted from 100 to 670 RPM. When the Graphite/Ethylene Glycol slurry was the lubricant, equivalent film thicknesses as the pure ethylene glycol were obtained and the above procedure was performed.

Temperature Results

The purpose of the thermister data was to determine the relation between the temperature difference at the inlet and

the edge of the bearing and the rotation speed (RPM). This experimental data were then compared with the mathematical predictions as developed in Chapter 4. The data shown in Figures 5-1 and 5-2 closely match the predictions within the uncertainty. The repeatability was within experimental uncertainty.

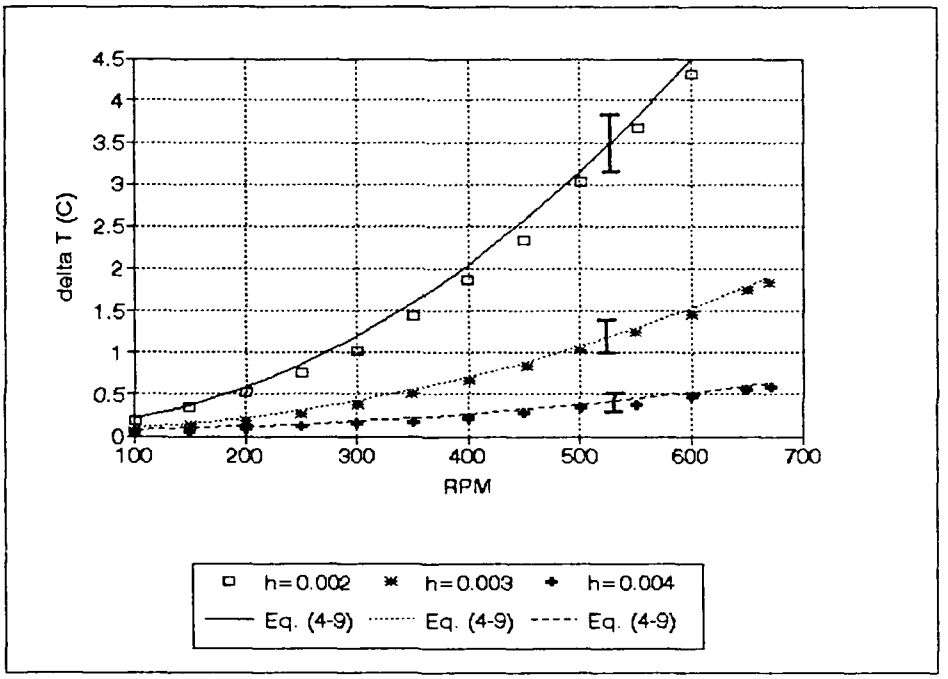

Figure 5-1. Ethylene Glycol Temperature Profile
Flow rate, h=0.002: 77 ml/min
h=0.003: 153 ml/min
h=0.004: 371 ml/min
Supply Pressure, h=0.002: 40 psi
h=0.003: 25 psi
h=0.004: 25 psi

Figure 5-2 clearly shows that the temperature difference at higher RPM for the graphite slurry is almost double the temperature difference shown in Figure 5-1 at

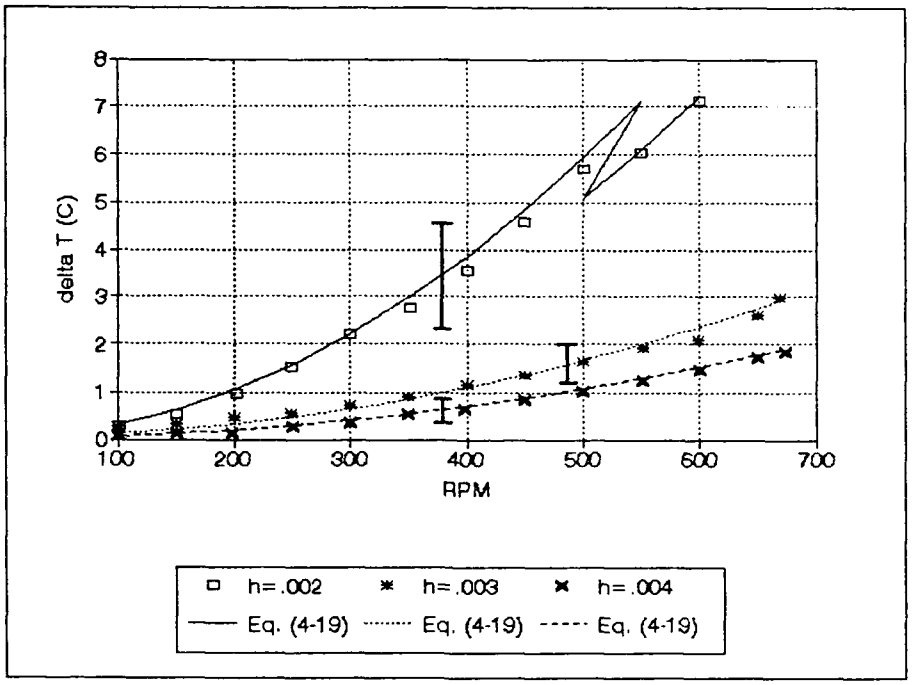

Figure 5-2. Graphite/Ethylene Glycol Temperature Profile

- Flow rate, h=0.002: 46 ml/min
  h=0.003: 114 ml/min
  h=0.004: 136 ml/min
- Supply Pressure, h=0.002: 40 psi
  h=0.003: 30 psi
  h=0.004: 15 psi

equal RPM and film thickness for the Newtonian fluid, ethylene glycol. It is especially prevalent for the 0.002 inch film thickness. This demonstrates that the presence of the graphite powder, thus making the fluid non-Newtonian, greatly increases the temperature change. For a rotating bearing with microstructures in the lubricant, the increase in temperature and subsequent power loss is expected due to an increase in the shear stress (15, p. 106). As discussed

in Chapter 4, the Power Law constants are dependent upon temperature. The values used for the rotation speed up to 500 RPM corresponded to temperature readings within the 30°C range. When the rotation exceeded 500 RPM, the temperature readings were higher and fell within the 40°C range. Therefore, the Power Law constants were adjusted resulting in the discontinuity shown in the theoretical curve in Figure 5-2 at h=0.002 inches. The uncertainty for the data points was too small to plot. The uncertainty for the mathematical model was determined as discussed in Chapter 3 with equation (3-2).

Pressure Results

The purpose of the pressure data was to determine the relationship between the pressure profile and the rotation speed (RPM). The inertial and temperature effects on the pressure are assumed to be negligible when compared to the shear stress. It has already been shown that the addition of the graphite particles increases the pressure at lower flow rates thus, increasing the load capacity of the hydrostatic step bearing (8, p. 33; 14, p. 16; 15, p. 106; 16, pp. 32-33). The effect of rotation on the pressure ratio versus the radius ratio is shown in Figures 5-3

through 5-8. The measured data compared closely with the mathematical predictions as developed in Chapter 4 at the lower rotation speeds within the uncertainty.

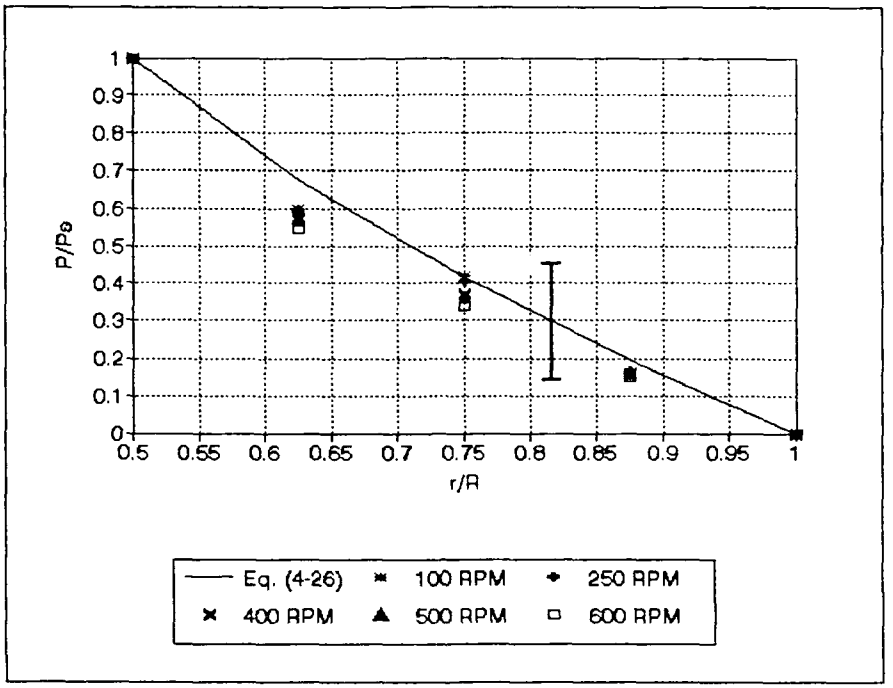

Figure 5-3. Ethylene Glycol Pressure Profile
◆ h=0.002; Flow rate=77 ml/min

The repeatability was within experimental uncertainty. The uncertainty for the data points was too small to plot. The uncertainty for the mathematical model was determined as discussed in Chapter 3 with equation (3-2).

The inlet pressure varied slightly during the course of the experimentation and therefore, the pressures were nondimensionalized by the appropriate supply pressure reading resulting in a pressure ratio of 1 at the step of

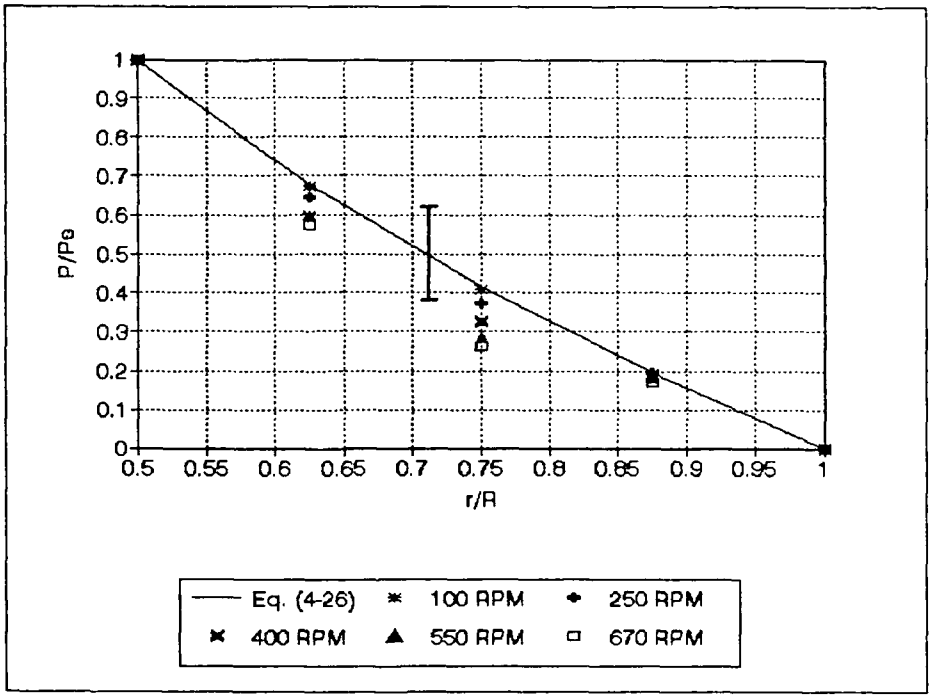

Figure 5-4. Ethylene Glycol Pressure Profile

◆ h=0.003; Flow rate=153 ml/min

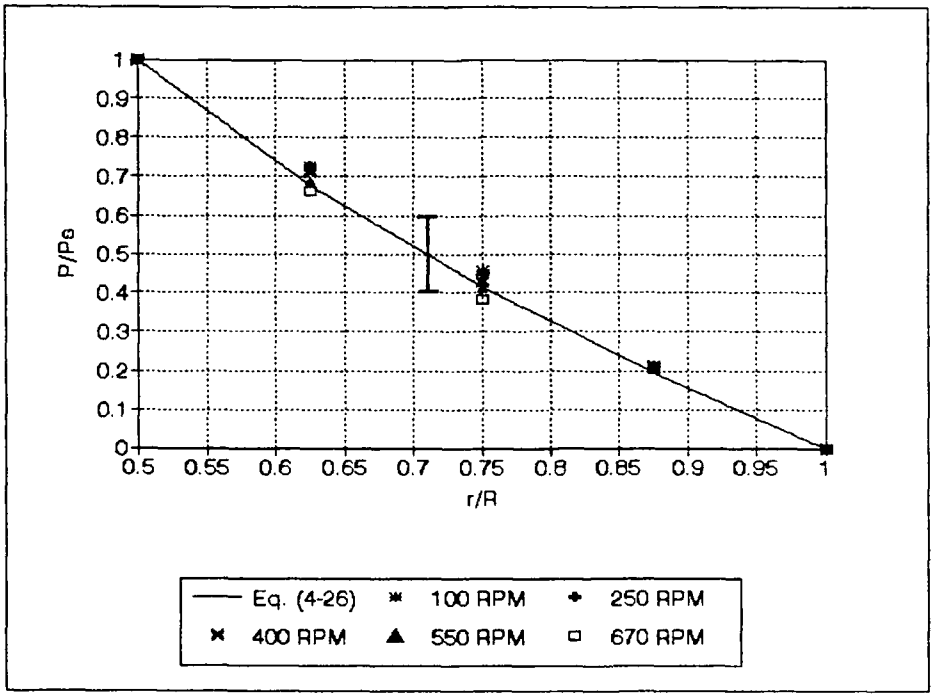

Figure 5-5. Ethylene Glycol Pressure Profile

◆ h=0.004; Flow rate=371 ml/min

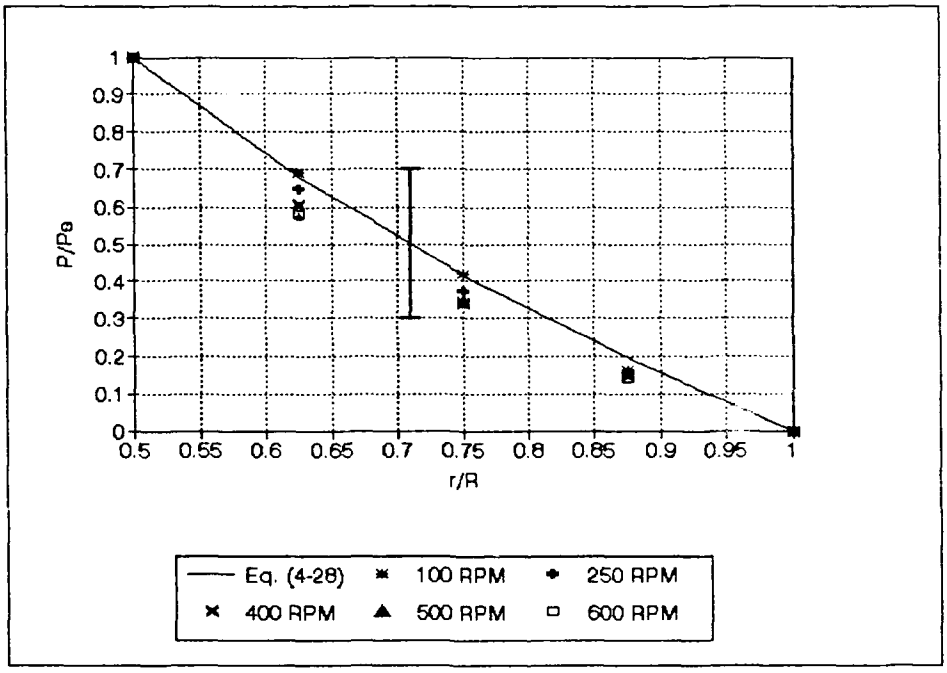

Figure 5-6. Graphite/Ethylene Glycol Pressure Profile

- h=0.002; Flow rate=46 ml/min

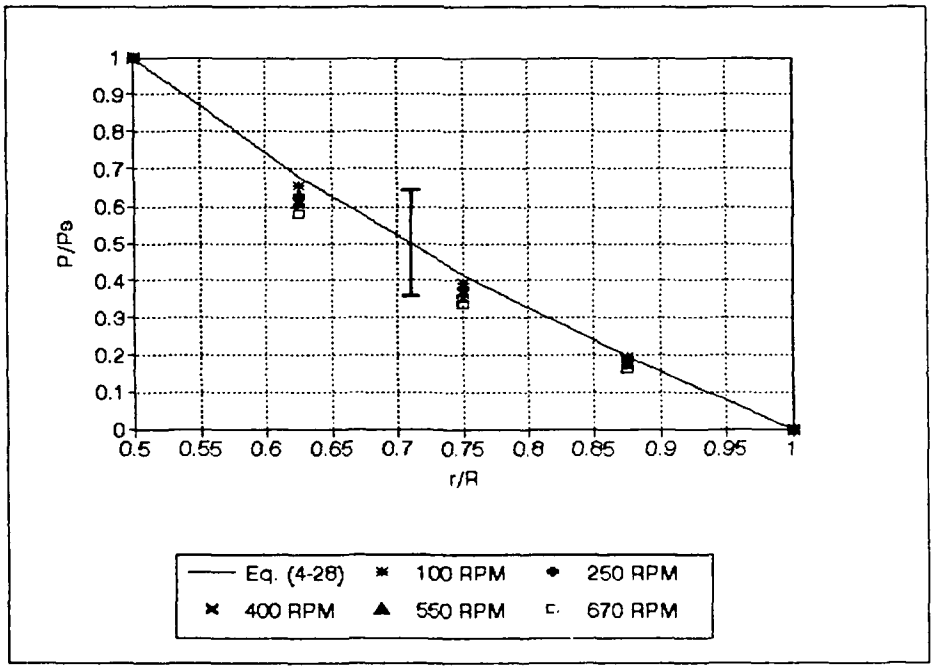

Figure 5-7. Graphite/Ethylene Glycol Pressure Profile

- h=0.003; Flow rate=114 ml/min

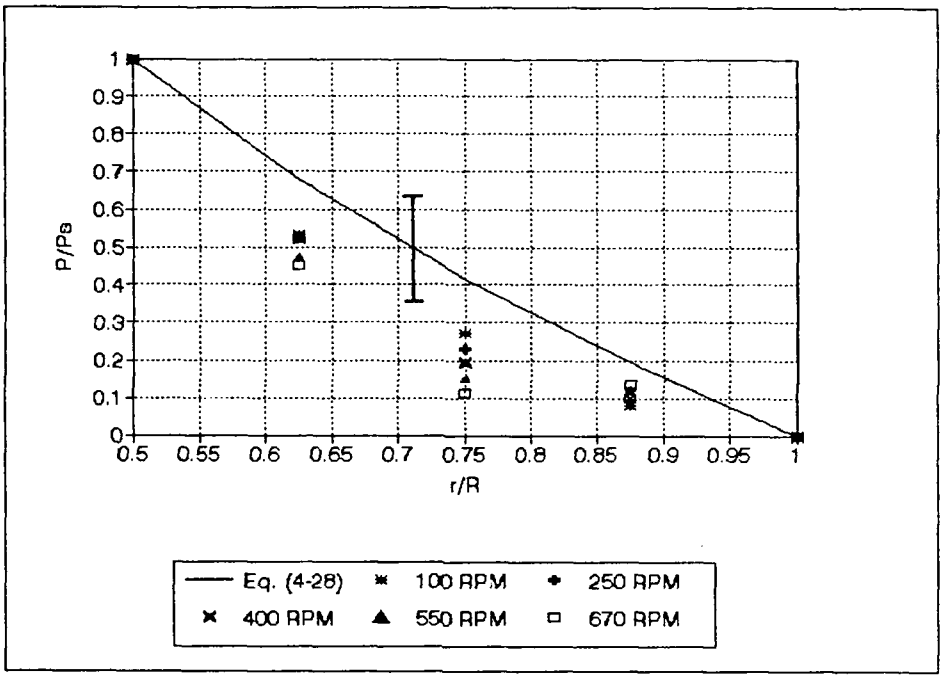

Figure 5-8. Graphite/Ethylene Glycol Pressure Profile

◆ h=0.004; Flow rate=136 ml/min

the bearing for each RPM value. The remaining pressure points were nondimensionalized by the same supply pressure.

The 100 RPM pressure ratios in Figures 5-3 and 5-5 varied slightly from the mathematical model, but are within the uncertainty. As shown in Figure 5-3, the increased speed resulted in a slight drop in the interior pressure readings whereas the two exit pressures did not vary appreciably. The probable reason for this decrease in pressure is due to the temperature dependency of the fluid viscosity. As noted in the previous results, the temperature of the bearing increased due to the raised

frictional loss at the higher rotations. As temperature increases, the viscosity becomes smaller resulting in a smaller pressure ratio. This decrease in pressure is also indicated in Figures 5-4 and 5-5. Preliminary temperature measurements of the interior of the bearing showed higher temperatures than those observed at the inlet or outlet points of the fluid flow emphasizing the presence of a greater temperature affect on the interior pressure reading than the outlet readings. The non-Newtonian pressure behavior shown in Figure 5-6 also indicates a drop in the pressure ratio. This decrease in the pressure ratio is larger than shown for an equal film thickness and RPM of the ethylene glycol in Figure 5-3. These results are further supported by comparing Figures 5-7 and 5-8 to their ethylene glycol counterparts, Figures 5-4 and 5-5. As shown in Table 4-1, the Power Law constants for the graphite/ethylene glycol slurry are also temperature dependent. Therefore, the non-Newtonian graphite slurry is also temperature dependent. The graphite slurry demonstrated a higher pressure drop than the Newtonian fluid, ethylene glycol, because of the higher temperatures shown in Figures 5-1 and 5-2 and discussed previously.

The decrease in pressure is significant because it translates to a loss of load carrying capability of the bearing. The higher load carrying capacity of the non-Newtonian lubricant is one of the reasons for their use. The pressure is still higher than the Newtonian lubricant, but it must be considered because the change in temperature experienced at extreme rotations will be substantially higher than Newtonian lubricants resulting in a higher pressure loss.

CHAPTER 5
CONCLUSIONS

The objective of this research was to determine the effects of adding a powder lubricant to a Newtonian carrier fluid on the lubrication temperature and pressure profile. The effects were shown through result comparisons between the pure ethylene glycol and the Graphite/Ethylene Glycol slurry.

A detailed uncertainty analysis of the measuring devices was undertaken to determine deviations between measured and predicted data.

Results compared favorably with the mathematical models.

The data presented agreed with the theoretical predictions based upon the rheological properties obtained from previous papers. These agreements give a high level of confidence for the use of the equations derived in this paper.

It was noted that the pressure profile of the graphite slurry was affected more by the higher rotations than the

pure Newtonian fluid. This affect can be expected due to the higher shear rate and subsequent temperature increase. Since viscosity of the graphite slurry is temperature dependent and the potential applications involve a significant increase to the rotation speed, it is recommended that further research should be conducted to study the interior temperature gains and their affect on the pressure profile of the bearing. Measuring the temperatures of the interior of the bearing in conjunction with the Power Law constants' curve fit as functions of temperature could result in a complete understanding of the pressure profile of a hydrostatic step bearing subjected to a rotation.

Preliminary testing showed that the temperature inside the bearing is higher than those noted at the inlet or outlet of the fluid flow. Therefore, any attempt to mathematically model the temperature dependency of the viscosity or the Power Law constants would have been inaccurate.

Another factor that could be present at significantly higher rotation speeds than those tested in this research is possible inertial effects of the graphite powder in the slurry mixture. That effect was not apparent in this

research since an increase in the pressure profile would be expected for such an occurrence.

The advantages of the non-Newtonian lubricant are their increased viscosity and subsequent higher load carrying capacity and their ability to operate at higher temperatures. However, when the bearing is operated at high rotation speeds, the higher shear rate creates an increased temperature which could have a weakening affect on their pressure profile. This affect would limit their load carrying capacity, although it still exceeds the capacity of the Newtonian lubricant. This thesis has shown the fundamental lubrication principles of a graphite slurry non-Newtonian fluid that was pressure induced into a rotational hydrostatic step bearing. Further investigations into higher rotation speeds and interior temperature gain are recommended to more fully understand the non-Newtonian behavior of the graphite/ethylene glycol lubricant.

REFERENCES

1. Rowe, W.B. "Advances in Hydrostatic and Hybrid Bearing Technology." Proceedings of the Institution of Mechanical Engineers. Part C, Journal of Mechanical Engineering Science. Volume 203, 1989, pp. 225-242.

2. Dowson, D. History of Tribology. London and New York: Longman Group Limited, 1979.

3. Franklin Institute Research Laboratories. NASA Contributions to Fluid-Film Lubrication. Technology Utilization Division, National Aeronautics and Space Administration. Washington, D.C.: Government Printing Office, 1969.

4. Fuller, D.D. Theory and Practice of Lubrication for Engineers. Second Edition. New York: John Wiley & Sons, 1984.

5. Campbell, M.E., J.B. Loser and E. Sneegas. Solid Lubricants. Technology Utilization Division, National Aeronautics and Space Administration. Washington, D.C.: Government Printing Office, 1966.

6. Campbell, M.E. Solid Lubricants. Technology Utilization Division, National Aeronautics and Space Administration. Washington, D.C.: Government Printing Office, 1972.

7. Dareing, D.W., and R.D. Dayton. "Non-Newtonian Behavior of Powder Lubricants Mixed with Ethylene Glycol." Society of Tribolgy and Lubrication Engineers. Tribology Transactions. Volume 35, 1992, pp. 114-120.

8. Wu, Z. "Non-Newtonian Effects of Powder-Lubricant Slurries in Hydrostatic and Squeeze Film Bearings." Master's Thesis, University of Florida, Gainesville, 1992.

9. Taylor, J.R. An Introduction to Error Analysis. Mill Valley, California: University Science Books, 1982.

10. Moffat, R.J. "Describing the Uncertainties in Experimental Results." Experimental Thermal and Fluid Science. Volume 1, 1988, pp. 3-17.

11. Moffat, R.J. "Contributions to the Theory of Single-Sample Uncertainty Analysis." Journal of Fluids Engineering. Volume 104, June 1982, pp. 250-260.

12. White, F.M. Fluid Mechanics. New York: McGraw-Hill Book Company, 1979.

13. Buckholz, R.H. "Effects of Power-Law, Non-Newtonian Lubricants on Load Capacity and Friction for Plane Slider Bearings." Journal of Tribology. Volume 108, January 1986, pp. 86-91.

14. Dareing, D.W. "Non-Newtonian Effects of Powder Lubricant Slurries in Hydrostatic and Hydrodynamic Bearings." Final Report, Air Force Office of Scientific Research, Contract F49620-88-C-0053/SB5881-0378. University of Florida, 1991.

15. Khader, M.S., and R.I. Vachon. "Theoretical Effects of Solid Particles in Hydrostatic Bearing Lubricant." Journal of Lubrication Technology. Volume 95, January 1973, pp. 104-106.

16. Najji, B., B. Bou-said and D. Berthe. "New Formulation for Lubrication with Non-Newtonian Fluids." Journal of Tribology. Volume 111, January, 1989, pp. 29-34.

APPENDIX SAMPLE UNCERTAINTY CALCULATION

Determining the uncertainty in the film thickness, equation (3-9), was accomplished through the use of equation (3-10) which is expanded as follows:

$$\omega_h = \left[\left(\frac{\partial h}{\partial y_A} \omega_{y_A} \right)^2 + \left(\frac{\partial h}{\partial y_B} \omega_{y_B} \right)^2 + \left(\frac{\partial h}{\partial y_C} \omega_{y_C} \right)^2 \right]^{\frac{1}{2}}$$

Substituting the values of the partial derivatives of equation (3-9) and the uncertainties of each LVDT results:

$$\omega_h = \left[(-.0022(\pm.04))^2 + (-.0025(\pm.07))^2 + (-.0033(\pm.05))^2 \right]^{\frac{1}{2}}$$

$$\omega_h = \pm 0.00026 \approx \pm 0.0003$$

This is the uncertainty stated on page 16 and demonstrates the procedure followed for all the uncertainty calculations.

BIOGRAPHICAL SKETCH

I am currently a Lieutenant in the Civil Engineer Corps of the United States Navy. I was born on May 3, 1964, in Monterey, California. I have lived in Fairborn, Ohio; Virginia Beach, Virginia; Orange Park, Florida; and Fairfax, Virginia.

I received a Bachelor of Science in Mechanical Engineering from the United States Naval Academy in May 1986. I was assigned for 3 years to the Naval Air Station in Jacksonville, Florida, and handled over $40 million in construction and repair projects. In 1989, I was transferred to Naval Mobile Construction Battalion 133, completing deployments to Guam; Rota, Spain; and northern Iraq as a company commander and officer-in-charge.

I transferred to the University of Florida in December 1991, completing the requirements for a Master of Science in mechanical engineering in December 1992. My next duty station is at the Navy Public Works Center in Pearl Harbor, Hawaii.